Journal of Non-Crystalline Solids 473 (2017) 26–32

Contents lists available at ScienceDirect

Journal of Non-Crystalline Solids

journal homepage: www.elsevier.com/locate/jnoncrysol

Analysis of TNM model calculation for enthalpy relaxation based on the fictive temperature model and the configurational entropy model

Yutaka Tanaka[a,*], Noriki Sakamoto[b]

[a] Department of Materials Science and Biotechnologies, University of Fukui, Bunkyo, Fukui 910-8507, Japan
[b] Department of Materials Science and Engineering, Faculty of Engineering, University of Fukui, Bunkyo, Fukui 910-8507, Japan

ARTICLE INFO

Keywords:
Glass transition
Enthalpy relaxation
Polystyrene
Fictive temperature
Configuration entropy
DSC

ABSTRACT

Enthalpy relaxation experiments were conducted for polystyrene samples at different annealing temperatures below glass transition temperature (T_g) using a differential scanning calorimeter. The framework of Tool-Narayanaswamy-Moynihan approach was applied to reproduce experimental traces with two models of the structural relaxation times; those are the generalized Arrhenius type characterized by fictive temperature (T_f model) and the configurational entropic type (S_c model). The calculation data of the heat capacity (c_p) obtained from the two models were analysed on the basis of the parameter – geometry relationship, in which three factors were given to the geometry of the T_g shoulder and overshoot appeared in c_p curve. It was found that both the horizontal shift and the broadening of T_g shoulder occur interdependently in the c_p curve calculation of S_c model, while they are almost independent in the calculation of T_f model. In addition, the analysis revealed the process of producing c_p overshoot in T_g shoulder, which is expected to be instructive in the optimized c_p calculation.

1. Introduction

Currently, the structural relaxation behaviour accompanied by the glass transition of polymer is mostly realized in terms of phenomenological models, as their increased flexibility allows suitable representation of most basic relaxation features of non-linearity [1], non-exponentiality [2–3], hysteresis [4] and thermorheological simplicity/complexity. The framework of Tool-Narayanaswamy-Moynihan (TNM) takes a leading role on this matter, even though some controversial points are remained over the ability to reproduce various properties for well-annealed polymer. Among various properties, we are interested in reproducing $c_p(T)$ curve, specific heat capacity, acquired by heating scan of DSC (differential scanning calorimetry) technique. A lot of research works can be seen in literatures for the reproduction of $c_p(T)$ including the enthalpy relaxation of inorganic glasses, where the strong correlation is shown between DSC temperature programme and the magnitude of enthalpy overshoot located near glass transition shoulder [5–17].

In the analysis of this correlation, the heating rate for scanning and the cooling rate before scanning are taken into consideration in the temperature programme. As a result of earlier works seen in literatures, it has been ascertained experimentally that the magnitude of enthalpy overshoot increases as the decrease in magnitude of cooling rate under the constant heating rate. At the same time, the position of the overshoot shifts towards higher temperature.

Previously, we have given three factors to the geometry of $c_p(T)$ curve in an attempt to account for the height and the position of overshoot: ⟨1⟩ position of glass transition shoulder, ⟨2⟩ width of glass transition shoulder, and ⟨3⟩ height of the overshoot [18], see Fig. 1. Needless to say, perfect simulations in the details of $c_p(T)$ are not realized by these factors only. However, they are useful in examining similarity/dissimilarity between several data observed under different technique and different temperature programs as written below.

Some supplementary explanation would help us grasp the tendency towards larger overshoot as the decrease in magnitude of cooling rate. The three most common temperature programs and thus thermal histories applied to the glassy polymer are mentioned regarding the experiment of enthalpy relaxation, after the schematic diagram shown by Svoboda et al. [7]: (a) the classic cycles, (b) intrinsic cycles, and (c) annealing cycles. In the classic cycles, the sample is repeatedly cooled from high temperature where any thermal histories are erased through T_g (glass transition temperature) at various cooling rates (Q_c), while the rate of heating scans (Q_h) are usually constant. The intrinsic cycles are similar to the classic cycles, except that the cooling-to-heating ratio (Q_c/Q_h) remains constant. The cycles in which the magnitudes of cooling and heating steps are same, are frequently seen in the experiment. In the annealing cycles, the isothermal stages are inserted during the cooling steps, where the annealing temperature and time are T_A and

* Corresponding author.
E-mail address: tanaka@matse.u-fukui.ac.jp (Y. Tanaka).

http://dx.doi.org/10.1016/j.jnoncrysol.2017.07.023
Received 9 March 2017; Received in revised form 5 July 2017; Accepted 25 July 2017
Available online 05 August 2017

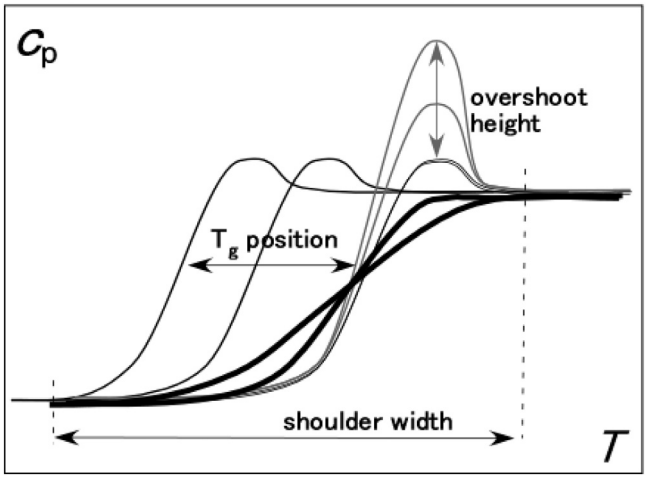

Fig. 1. Schematic illustration for the three factors given to the geometry of $c_p(T)$ curve in an attempt to account for the height and the position of overshoot: ⟨1⟩ position of glass transition shoulder, ⟨2⟩ width of glass transition shoulder, ⟨3⟩ height of the overshoot.

t_A respectively, afterwards the heating scans are conducted.

Fairly characteristic T_g shoulder and overshoot appear in the c_p curve in response to Q_c and/or t_A of these temperature programs. It is necessary to rationalize these responses by following the time constant (τ) of the structural relaxation and the equations utilized in TNM framework. As for the relaxation time, a detailed summary can be found in a literature in which it is described in association with non-linearity and non-exponentiality of the evolution towards the equilibrium [1]. Many experimental and calculation data are discussed there with examining several formulae, in an attempt to find a suitable description for τ or to seek for effective methods to predict $c_p(T)$ curve. The generalized Arrhenius form of Eq. (1) appears most frequently,

$$\tau = A\exp\left(\frac{x\Delta h^*}{RT} + \frac{(1-x)\Delta h^*}{RT_f}\right) \quad (1)$$

where $0 < x \leq 1$, Δh^* is the activation energy, R gas constant, T and T_f are actual and fictive temperature, respectively. The expression based on the configurational entropy also offers a promising approach, which originates from the Adam-Gibbs theory of the relaxation in glass-forming liquids [19].

$$\tau = A\exp\left(\frac{B}{TS_c}\right) \quad (2)$$

where S_c is configurational entropy and B the energy constant.

Accordingly, several parameters such as A, x, Δh^* in Eq. (1) and A, B in Eq. (2) are utilized in the TNM framework to obtain the $c_p(T)$ calculation data; the calculations using Eqs. (1) and (2) are referred to as those of T_f model and S_c model in this work. The model calculation is, in practice, carried out through a fine tuning of these parameters, i.e. the value of each parameter is varied step by step, to produce a $c_p(T)$ curve of an appropriate geometry factors where calculation data coincides with the experimental data. Therefore, to grasp the relationship between the parameter and the geometry is highly important for understanding the response of $c_p(T)$ curve to the temperature programme and conducting the optimized calculation. The parameter–geometry relationship is also meaningful for considering the suitable expression of τ among the equations of the relaxation time.

In order to clarify this relationship, we gave the calculation curves based on both T_f model and S_c model to fit with the experimental $c_p(T)$ data of amorphous polystyrene with the annealing cycle. Although the proposals of the glass transition kinetics can be seen other than Eqs. (1) and (2), these are focused on in this work by taking account of the effectiveness of the natural separation of actual and fictive temperature. Experimental data of many different relaxation phenomena have already been presented for polystyrene by several research groups [20–24]. The derived value in the parameter–geometry relationship was examined not to be inconceivable with reference to these previous relaxation data. Next, it was attempted to find any parameters which variation causes the change in geometry of the three factors of ⟨1–3⟩. It was revealed in the process of these analyses on T_f model that the result of the variation of the effective parameter is well illustrated in the plot of T_f vs T. Furthermore, the retardation function, a constituent term of the TNM framework has a central role in the analysis of this relationship. It is conceivable that the acquired knowledge is instructive in the optimized calculation for $c_p(T)$ curve of the annealing cycle.

2. Methodology

2.1. Materials

Polystyrene (PS) pellet was purchased from Wako Pure Chemical Industries, Ltd. $M_w = 1.01 \times 10^5$, $(M_w/M_n) = 1.54$, which values were determined by GPC (GL-Science, Ltd. Model557 and RI504R) calibrated with the standard polystyrene samples. Polystyrene powder was prepared from the pellets via precipitation with methanol from solution in THF. $T_g = 102$ °C which value was determined using the onset of glass transition shoulder appeared in the heat flow curve.

2.2. DSC measurements

The heat capacity, $c_p(T)$, of Wako polystyrene were obtained from the heat flow curve using SEIKO DSC200 with aluminum open sample pans of 5ϕ. The calibration was carried out with reference to c_p of Indium of −23.15 °C, 24.85 °C, 126.85 °C. The ageing experiments were conducted in DSC measurements, in which Wako polystyrene was (i) first maintained at 160 °C, approximately (T_g + 60 °C) for 5 min to erase thermal history; (ii) cooled to a specified ageing temperature, T_A with a cooling rate of 12 °C/min; (iii) annealed for the ageing period t_A; and (iv) cooled to a temperature well below T_g (approximately T_g − 80 °C); then the heat flow curve was recorded on heating with a rate of 5 °C/min. The enthalpy loss during the annealing was indicated as ΔH (t_A, T_A). Other details for the measurement are described in previous works [25].

2.3. Model calculations

The brief description concerning T_f and S_c models employed in this work was given to clarify variables used. More equations, variables and valuable suggestions appear in the whole theory of reproducing $c_p(T)$ curve(see ref. 9, 6, and references cited therein).

The non-exponentiality of the relaxation function (ϕ) can be written by the stretched exponential form with the shape parameter of β ($0 < \beta \leq 1$).

$$\phi = \exp[-(t_A/\tau_0)^\beta] \quad (3)$$

ϕBefore fitting the measured $c_p(T)$ with the calculation data, the parameter β was determined using $\Delta H(t_A, T_A)$ measured in the annealing experiments of T_A = 84, 89, 94 °C; numerical data are shown in the later section. The relation between $\Delta H(t_A, T_A)$ and the relaxation function is written as Eq. (4) through $\Delta H(\infty, T_A)$ which is the limiting value for $t_A \to \infty$.

$$\Delta H(t_A, T_A) = \Delta H(\infty, T_A) \times (1-\phi) \quad (4)$$

T_f and/or S_c were used to quantify the structure of the sample in its non-equilibrium state as mentioned in Eqs. (1) and (2) [1,12]. The fictive temperature is the temperature at which the enthalpy of a given state, if extrapolated along the glass line, would intersect the equilibrium liquid line. Hence, T_f evolves from one limiting case to another through the glass transition on heating or cooling. This evolution of the fictive temperature can be calculated using T_f model. For any arbitrary

set of temperature scans starting initially in the equilibrium state at T_0, it can be calculated using the following equation [26]:

$$T_f = T_0 + \sum_{i=1}^{n} \Delta T_i \left\{ 1 - \exp\left[-\left(\sum_{j=i}^{n} \frac{\Delta T_j}{Q_j \tau_j} \right)^{\beta} \right] \right\} \quad (5)$$

where ΔT_i is the temperature change corresponding to the i–th step, and Q_j is the cooling rate or heating rate corresponding to the j–th step. The calculation yields T_f data which was converted to the heat capacity using Eq. (6) in order to compare the model with the experimental data:

$$c_p(T) = c_{pg}(T) + \Delta c_p(T_f) \frac{dT_f}{dT} \quad (6)$$

where $\Delta c_p(T_f)$ is the difference in the heat capacity between the liquid and glassy states evaluated at T_f. The glass and liquid heat capacities (c_{pg} and c_{pl}, respectively) were determined for each curve in the range from approximately T_g-10 °C to T_g-20 °C for the glassy state and from T_g + 10 °C to T_g + 20 °C in the liquid state.

In the investigation of the effect of Δh^* variation on c_p curve, it was found that the n-th term of $\Delta T_i[1 - \exp[- (\Sigma(\Delta T_j / Q_j \tau_j))^{\beta}]]$ in the summation of Eq. (5) plays a dominant role in calculating T_f. This n-th term divided by ΔT_i was then defined as $G(T)$, that is the retardation function in the element of Boltzmann constitutive equation, and examined minutely in this work. It follows that $0 < G(T) < 1$ when Q_j and τ_j varies independently.

In S_c model, the evolution of the configurational entropy in response to a thermal history that consists of a series of temperature jumps from T_{i-1} to T_i at time instant t_i followed by isothermal stages is given by,

$$S_c(t) = S_c^{\lim}[T(t)] - \sum_{i=1}^{n} [S_c^{\lim}(T_i) - S_c^{\lim}(T_{i-1})] \times \exp\left[-\left(\sum_{j=i}^{n} \frac{\Delta T_j}{Q_j \tau_j} \right)^{\beta} \right] \quad (7)$$

If the limit state of the structural relaxation process coincides with the extrapolation of the equilibrium values determined at temperatures above T_g, $S_c^{\lim}(T) = S_c^{eq}(T)$ can be given with,

$$S_c^{eq}(T) = \int_{T_2}^{T} \frac{\Delta c_p(\theta)}{\theta} d\theta \quad (8)$$

where $\Delta c_p(T) = c_{pl}(T) - c_{pg}(T)$ is the difference in the heat capacity between equilibrium liquid and glass at same temperature. T_2 is the 2nd order transition temperature. Further, the limiting value of $\Delta c_p(T)$ can be written as $\Delta c_p^{\lim}(T) = c_{pl}^{\lim}(T) - c_{pg}(T)$, and then $S_c^{\lim}(T)$ is calculated as,

$$S_c^{\lim}(T) = S_c^{eq}(T^*) + \int_{T^*}^{T} \frac{\Delta c_p^{\lim}(\theta)}{\theta} d\theta \quad (9)$$

T^* is a temperature above T_g, where the limit state coincides with the equilibrium state. $T^* = T_g + 10$ °C was taken in this study after the manner shown by Gómez et al. [15,16].

By applying a set of these equations to the thermal history, the expression of $S_c(t)$ is obtained.

$$S_c(t) = S_c^{\lim}[T(t)] - \sum_{i=1}^{n} \left(\int_{T_{i-1}}^{T_i} \frac{\Delta c_p^{\lim}(\theta)}{\theta} d\theta \right) \times \exp\left[-\left(\sum_{j=i}^{n} \frac{\Delta T_j}{Q_j \tau_j} \right)^{\beta} \right] \quad (10)$$

The calculation of $c_p(T)$ was conducted using the following equation,

$$c_p(T) - c_{pg}(T) = dH_c/dT \quad (11)$$

where H_c is the specific configurational enthalpy. For the dependence of H_c on the thermal history, the same manipulation as used for $S_c(t)$ is applied. The assumption made here in order to determine H_c is that the enthalpy and entropy have the same relaxation function; in other words, the relaxation times for enthalpy decay and entropy decay are same.

The calculation data were derived with both T_f and S_c models and used for the fitting procedure with the aim reproducing five different DSC curves obtained for the thermal history of the constant annealing temperature (the number of DSC curves varied depending on the set of measurements). The temperature step size was chosen as 0.1 °C on cooling and heating rates, which was taken after the method used in a literature [10]. T_f model contains adjustable parameters of A, x and Δh^*, S_c model, those of of A, B and T_2; in the calculation of Eq. (5) and/or Eq. (10), ln(A) was used in practice instead of A. An iterative search routine for these parameters were used to determine the best set to reproduce heat capacity data with reference to the method of function minimisation [27]; the successive substitutions of the parameters were carried out to find the minimum of the average square deviation defined by Eq. (12).

$$\sigma_{ave} = \frac{1}{5N} \sum_{j=1}^{N} \sum_{i=1}^{5} w(i)[c_{exp}(i,j) - c_{cal}(i,j)]^2 \quad (12)$$

The index i means the experimental scan number while the index j denotes the points of each scan.

3. Results

Fig. 2 shows $c_p(T)$ curves acquired by the annealing experiments of T_A = 84, 89, 94 °C, which have a typical relaxation behaviour that larger enthalpy decay appears at lower T_A and longer t_A. In addition, the temperature of the endothermic peak shifted higher with the annealing time. Because the peak temperature corresponds to the process of recovery of enthalpy during the heating of the aged sample, the shift of peak temperature is due to the decrease of the molecular mobility of polystyrene chain segments as a consequence of the decrease in the free volume [28]. The equivalence between the energy absorbed during heating through the glass transition and the enthalpy loss associated

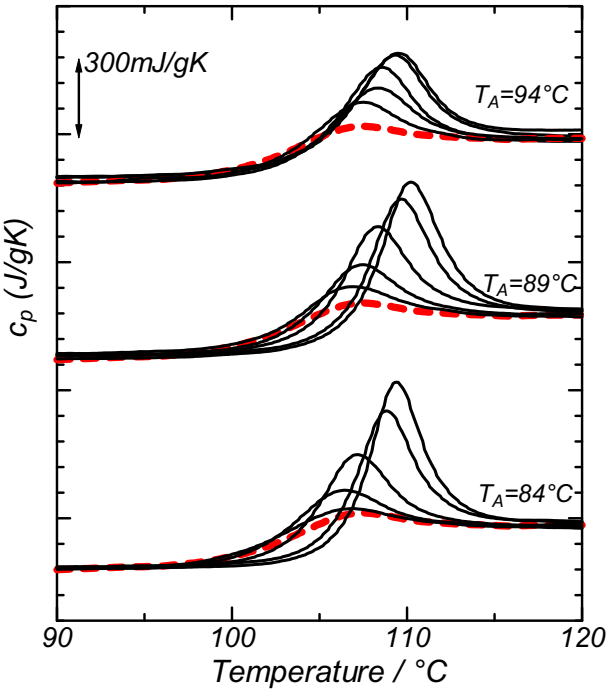

Fig. 2. Heat capacity data acquired by the annealing experiments of T_A = 84, 89 and 94 °C for Wako polystyrene samples. The annealing times (t_A) were 22, 80, 278, 1007, 1908 min in order of decreasing intensity. Data of t_A = 0 were also shown by thick dashed lines.

Table 1
List of parameters characterizing the relaxation function of Eqs. (3) and (4).

T_A/°C	$T_g - T_A$	ΔH_∞/Jg^{-1}	τ/min	β
84	18	2.790	9709	0.281
89	13	2.015	1874	0.311
94	8	1.240	107	0.330

with the isothermal annealing is well established. Hence $\Delta H(t_A, T_A)$ was evaluated from the area bounded by $c_p(T)$ curves with and without ageing; which data was fitted with Eqs. (3) and (4) to determine $\Delta H(\infty, T_A)$, τ_0 and β (see Table 1). β values obtained in this work showed some temperature dependence, which may be acceptable, although the temperature dependence of β was barely seen in the literature [29].

The results of the data fitting between experimental and calculated $c_p(T)$ of $T_A = 89$ °C using both T_f model and S_c model are shown in Fig. 3. The parameters used for the curve fittings are as follows; $\ln(A) = -369$, $\Delta h^* = 1166$ kJ/mol K, $x = 0.76$ for T_f model calculation, $\ln(A) = -25$, $B = 210$ J/g, $T_2 = 54.5$ °C for S_c model calculation, which are referred to as the best fitting values. As can be seen in Fig. 3, there was not much difference between the calculations using T_f and S_c models in the reproducibility of the experimental data. However, following the results of data fitting, several important features came out for the two models as described below, by exploring the relationship between the geometry of $c_p(T)$ curve and the variation of model parameters.

4. Discussion

4.1. Calculation curve of T_f model

As a result of the examination of the parameter–geometry relationship of T_f model which has three parameters of x, Δh^* and $\ln(A)$ in the calculation, it was found that the shoulder shifts to higher temperature side with the decrease in $\ln(A)$ along the baseline of $c_{pg}(T)$, and that the transition shoulder broadened with the decrease in Δh^*. These two geometrical factors of ⟨1⟩ and ⟨2⟩ have come out with the parameters near the best fitting values shown above. The relationship between the shoulder shift and $\ln(A)$ is displayed for $c_p(T)$ of $T_A = 89$ °C, $t_A = 0$, in Fig. 4(c) with varying $\ln(A)$ from −387 to −367. Plots of T_f vs T and $G(T)$ vs T are also shown in Fig. 4 to follow the shoulder shift of $c_p(T)$ curve. The calculation was conducted successively for the cooling and heating processes from 20 to 160 °C.

T_f decreases along the line of $T_f = T$ at high temperature on the cooling process, then departs from it in the transition region. On further cooling, T_f hardly decreases after the transition as shown in Fig. 4(a); in the different words, T_f almost remained at the plateau value and the difference between T_f and real temperature increases as the decrease in T. The value of T_f at the end of cooling process was defined as T_{f_start} because it really means the value at the start of heating and has significance for the shift of T_g shoulder.

The result that T_{f_start} increases as the increase in $\ln(A)$ is understandable when the summation of $(\Delta T_j/Q_j\tau_j)$ is considered. Because x and Δh^* are not varied in Eq. (1), τ increases as the increase in $\ln(A)$, which brings about the decrease in $(\Sigma(\Delta T_j / Q_j\tau_j))^\beta$ in Eq. (5). In consequence, the individual term decreases in the summation of $(1 - \exp[-((\Delta T_j / Q_j\tau_j))^\beta])$ and T_{f_start} increases. To elucidate this relationship more specifically, $G(T)$ is plotted against temperature in Fig. 4(b), where the decrease in the summation of $(1 - \exp[-((\Delta T_j / Q_j\tau_j))^\beta])$ with the increase in $\ln(A)$ can be seen as the horizontal shift of $G(T)$ vs T plot.

In the heating process, there is a plateau region of T_f at low temperature (see Fig. 4(a)), then T_f bends up to meet with the line of $T_f = T$ by heating. The hysteresis effect appears between cooling and heating, although it is little. This bend up corresponds to the T_g shoulder of $c_p(T)$ curve and shifts to higher temperature side as the increase in $\ln(A)$.

The bend up is meaningful to understand the relation between t_A of the annealing cycle and the $c_p(T)$ overshoot, and also the relation between the magnitude of the cooling rate in the classic cycle (Q_c) and the overshoot. The T_f vs T plots of the annealing cycle at $T_A = 89$ °C are shown in Fig. 5 to account for this relation; in the cooling process (Fig. 5(a)) T_f is lowered isothermally at 89 °C, which results in the decrease of T_{f_start}. The longer t_A, the larger decrease. For the annealed sample, the heating process begins with lower T_f than that of the unannealed (i.e., $t_A = 0$) sample. On the other hand, the recoveries of the fictive temperature due to heating before the bend up starts, are approximately same between the annealed and unannealed samples. As a result, T_f bends up after passing the line of $T_f = T$, that is, in the region of $T_f < T$ as shown in Fig. 5(b) for the sample having well lowered T_{f_start}. The rapid increase of T_f in the region of $T_f < T$ corresponds to the overshoot of $c_p(T)$ curve, and therefore the height of overshoot is determined by how much T_{f_start} is lowered from that of unannealed sample which is approximately measurable by t_A. As for the effect of the magnitude of Q_c in the classic cycle, the calculation results in this work evidenced that T_{f_start} becomes lower as the decrease in the magnitude and that T_f bends up more rapidly in the $T_f < T$ region by heating. It follows that the hysteresis effect between cooling and heating becomes more appreciable and $c_p(T)$ overshoot appears more significantly as the decrease in Q_c magnitude.

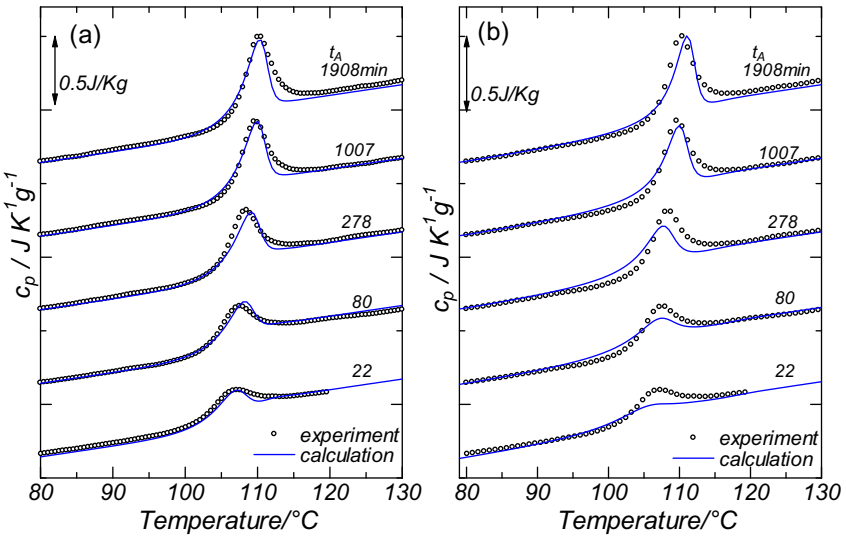

Fig. 3. The simultaneous fitting of $c_p(T)$ curves acquired for the annealing experiments of $T_A = 89$ °C for Wako polystyrene samples. (a) the fitting of T_f-model, (b) the fitting of S_c-model. Solid lines and circle plots are the calculation and experimental data respectively. The sets of model parameters used are shown in the text.

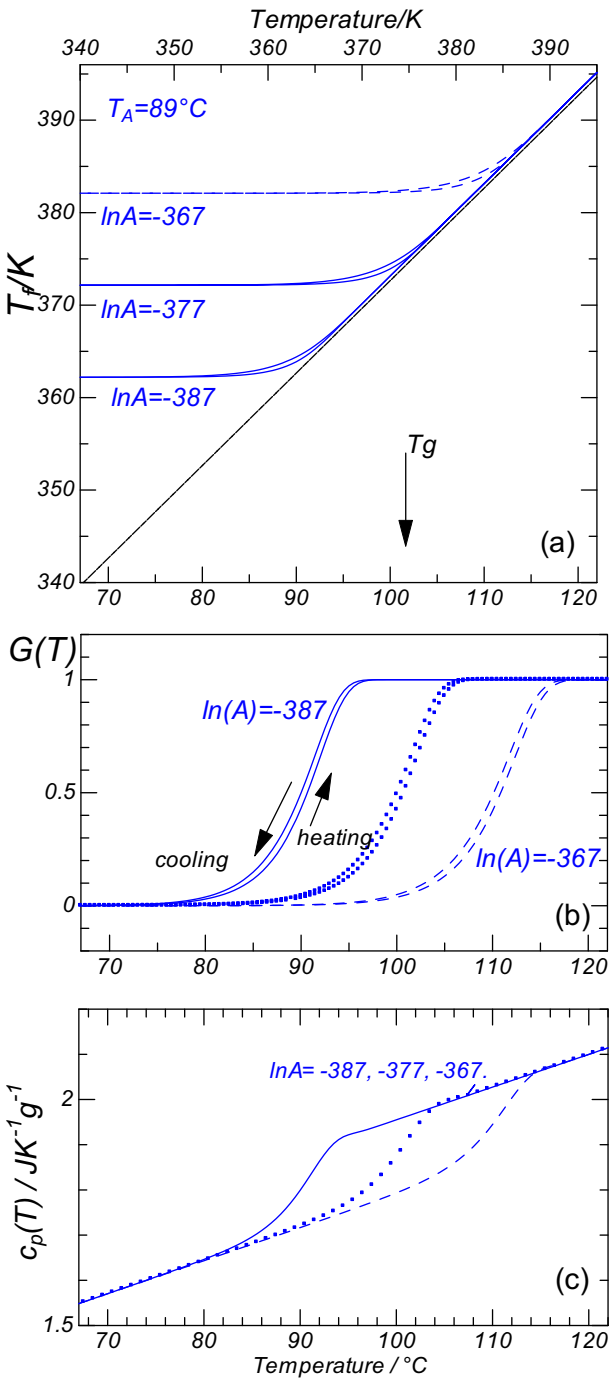

Fig. 4. T_f vs T and $G(T)$ vs T plots, (a) and (b) respectively, to account for the relationship between the shift of T_g shoulder and ln(A) variation at T_A = 89 °C, t_A = 0. Line of T_f = T was drawn in (a) for reference. Corresponding c_p curves are shown in (c). The plots are calculated with ln(A) = − 387 (solid line), − 377 (dotted line) and − 367 (dashed line) while x = 0.76, Δh^* = 1166 kJ/mol are fixed. The hysteresis is indicated with cooling and heating arrows in (b).

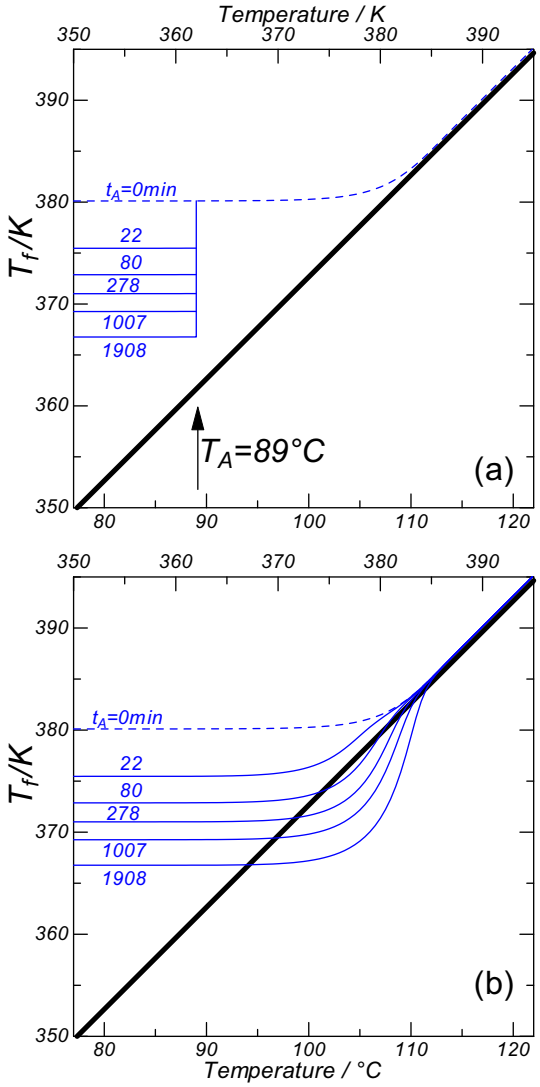

Fig. 5. T_f vs T of cooling process (a) and heating process (b), T_A = 89 °C, plotted to account for the decrease in $T_{f\text{-start}}$ with the increase in t_A which results in the increase of overshoot height in $c_p(T)$ curve. Parameters of ln(A) = − 369, x = 0.76, Δh^* = 1166 kJ/mol are used in the calculations.

Fig. 6(c) shows the relation between the variation of Δh^* and the broadening of transition shoulder in c_p curve; Δh^* was varied from 566 to 2966 kJ/mol with fixing ln(A)to be − 369, x to be 0.76. The plots of T_f vs T and $G(T)$ vs T are also displayed in Fig. 6(a) and (b), respectively. Δh^* = 566 kJ/mol is the lowest of the energy value examined, where the variation of RT is more sensitive to τ than that occurred against higher Δh^* according to Eq. (1); actually, RT is varied in the range of 293 < T < 433 K in the c_p calculation. Therefore, decrease in $G(T)$ starts at higher temperature in the cooling process and the increase starts at lower temperature in the heating process, which means a more broad transition region. As a result, the heating T_f vs T plot of Δh^* = 566 start to bend up at very low temperature to meet up with the line of T_f = T at high temperature. If Δh^* of a high value is used, the opposite mathematics proceeds in the c_p calculation. When Fig. 4(a) and Fig. 5(a) are compared, the increase in Δh^* should have an increasing effect on τ (see Eq. (1)), which does not actually lead well to the increase in T_{f_start} like ln(A) variation showed.

4.2. Calculation curve of S_c model

The parameter–geometry relationship of S_c model was examined by varying the three parameters of B, T_2 and ln(A). It was found that the T_g-shoulder shifts to higher temperature side with the decrease in ln(A). The shoulder shift was analysed by plotting the S_c vs T curve and the line of S_c^{eq} of Eq. (8), which was quite similar to the plot of T_f vs T constructed in T_f model, and by defining the S_c value at the starting of the heating process, i.e. S_c at 20 °C as $S_{c\text{-start}}$.

The value of $S_{c\text{-start}}$, and hence the difference between $S_{c\text{-start}}$ and S_c^{eq} at a given temperature well lower than T_g increased as the increase in ln(A) as shown in Fig. 7, where ln(A) is varied from − 32 to − 20

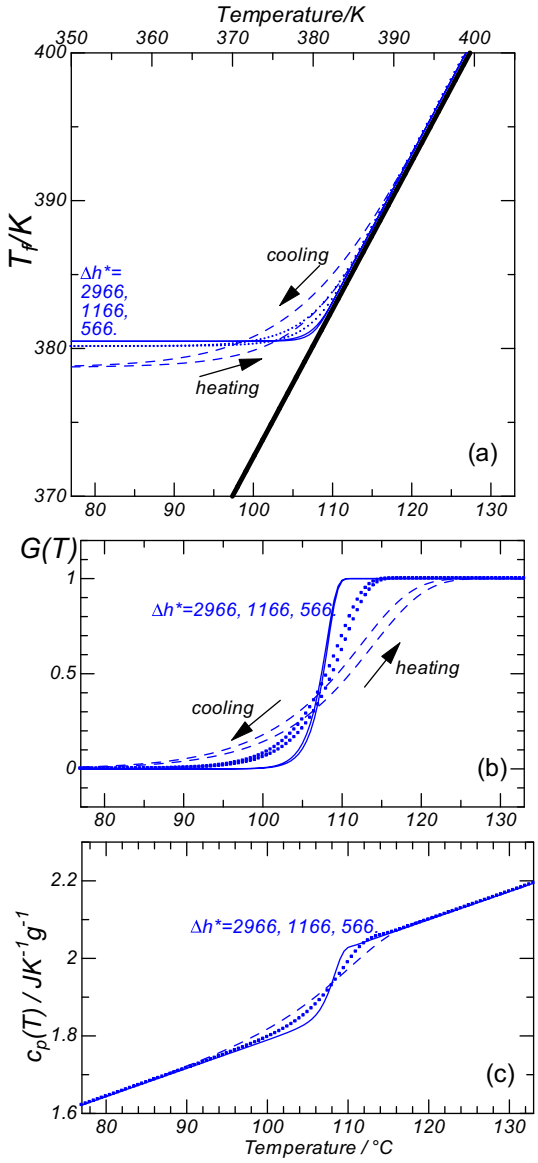

Fig. 6. T_f vs T, G_j vs T plots of (a) and (b) respectively, to account for the relationship between the broadening of T_g shoulder and Δh^*-variation at $T_A = 89$ °C, $t_A = 0$. Corresponding c_p curves are shown in (c). The plots are calculated with $\Delta h^* = 566$ (dashed), 1166 (dotted) and 2966 (solid), while $x = 0.76$, $\ln(A) = -369$ are fixed. The hysteresis is indicated with cooling and heating arrows in (b).

under $T_A = 89$ °C, $t_A = 0$. We have confirmed that the reason of the increase in $S_{c\text{-start}}$ is attributed to the increase in τ (see Eq. (2)). It was also found that the increase in the difference between $S_{c\text{-start}}$ and S_c^{eq} results in the shoulder shift towards higher temperature side in $c_p(T)$ curve. Furthermore, the effect of t_A in the annealing cycle has come out as the isothermal decrease in S_c at T_A, and hence the decrease in $S_{c\text{-start}}$ (see the plots of $t_A = 280$ and 1902 min in Fig. 7). These mechanisms are approximately same as those seen in the calculation of T_f model.

On the other hand, we could not observe such a distinct broadening of the shoulder as seen in the calculation of T_f model. That is, when B was varied with fixing T_2 and $\ln(A)$ to be the best fitting values written above, the broadening and the shoulder shift occurred simultaneously. More specifically, the shoulder shifted to higher temperature side and broadened with the increase in B. The broadening and shoulder shift also appeared together when T_2 was varied around the fitting value. It follows that the curve fitting of the factors ⟨1⟩ and ⟨2⟩ are mixed together in Fig. 2b) to produce the calculation data of S_c model. Accordingly, the effects of the variation of Δh^* in Eq. (1) and that of B in

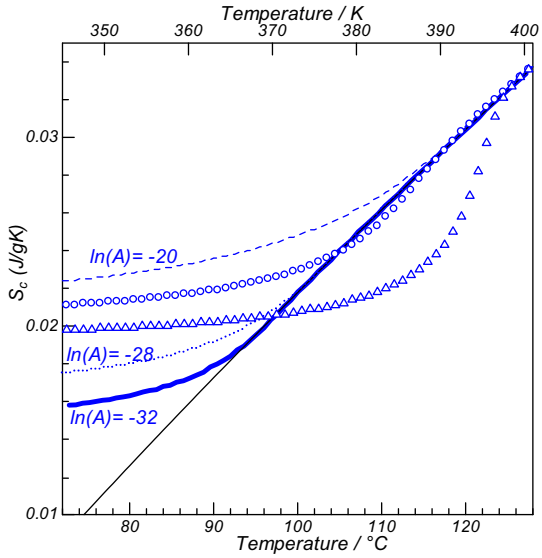

Fig. 7. Configuration entropy $S_c(t)$ plotted against temperature for the heating $c_p(T)$ data of the annealing experiment of $T_A = 89$ °C. Lines are those calculated with $\ln(A) = -20$ (dashed), -28 (dotted), -32 (solid) and $t_A = 0$ min. Plots are those calculated with ln (A) fixed to -20, $t_A = -278$ (circle), 1908 min (triangle). The thick solid line represents S_c^{eq} (T).

Eq. (2) appear in $c_p(T)$ curves with the different geometrical factor.

5. Concluding remarks

Concerning the enthalpy relaxation of polystyrene, both experimental and calculation data were presented for the annealing cycle. The calculation data were derived using T_f model and S_c model within the TNM framework, to reproduce the experimental result with the optimized fitting parameters of $\ln(A)$, Δh^* and x in T_f model and $\ln(A)$, B, T_2 in S_c model. In addition, by defining geometry factors to T_g shoulder in the experimental c_p curve, the parameter – geometry relationship, that is the variation of c_p curve against the variation of parameter was examined to acquire information on the curve fitting process in the calculation. In consequence, although the fitting power had no remarkable difference between the calculations of T_f and S_c models, the parameter – geometry relation is fairly different from each other. It is convenient to use T_f vs T and S_c vs T plots for seeing throughout the result of the parameter variation. The acquired knowledge about the calculation details is instructive in the optimized calculation for $c_p(T)$ curve of the enthalpy relaxation experiment.

Acknowledgement

In this work we used the supercomputer of ACCMS, Kyoto University, for the calculation of c_p(T) data.

References

[1] I.M. Hodge, Macromolecules 20 (1987) 2897.
[2] M. Goldstein, J. Chem. Phys. 39 (12) (1963) 3369–3374.
[3] A.J. Kovacs, J.J. Aklonis, J.M. Hutchinson, A.R. Ramos, J. Polym. Sci. Polym. Phys. Ed. 17 (1979) 1097.
[4] T. Divoux, V. Grenard, S. Manneville, Phys. Rev. Lett. 110 (2013) 018304.
[5] E.A. McGonigle, J.M.G. Cowie, V. Arrighi, R.A. Pethrick, J. Mater. Sci. 40 (2005) 1869.
[6] R. Svoboda, Acta Mater. 61 (2013) 4534.
[7] R. Svoboda, J. Málek, J. Non-cryst, Solids 378 (2013) 186.
[8] S.L. Simon, Macromolecules 30 (1997) 4056.
[9] P. Badrinarayanan, S.L. Simon, Polymer 48 (2007) 1464.
[10] P. Badrinarayanan, S.L. Simon, R.J. Lyng, J.M. O'Reilly, Polymer 49 (2008) 3554.
[11] Y.P. Koh, S.L. Simon, J. Polym. Sci. B Polym. Phys. 46 (2008) 2741.
[12] J.J. Tribone, J.M. O'Reilly, J. Greener, Macromolecules 19 (1986) 1732.
[13] J. Shin, S. Nazarenko, J.P. Phillips, C.E. Hoyle, Polymer 50 (2009) 6281.

[14] J. Shin, S. Nazarenko, C.E. Hoyle, Macromolecules 41 (2008) 6741.
[15] J.L. Gómez Ribelles, A. Ribes Greus, R. Díazor Calleja, Polymer 31 (1990) 223.
[16] J.L. Gómez Ribelles, M. Monleon Pradas, Macromolecules 28 (1995) 5867.
[17] L. Andreozzi, M. Faetti, M. Giordano, D. Palazzuoli, Macromolecules 35 (2002) 9049.
[18] Y. Okuya, N. Sakamoto, Y. Tanaka, Abstracts of 6th Pacific Rim Conference on Rheology, Melbourne, 228 (2014).
[19] G. Adam, J.H. Gibbs, J. Chem. Phys. 43 (1965) 139.
[20] A. Weitz, B. Wunderlich, J. Polym. Sci. Polym. Phys. Ed. 12 (1974) 2473.
[21] K. Adachi, T. Kotaka, Polym. J. 14 (1982) 959.
[22] R. Roe, G.M. Millman, Polym. Eng. Sci. 23 (1983) 318.
[23] E.F. Oleinik, Polym. J. 19 (1987) 105.
[24] S.L. Simon, J.W. Sobieski, D.J. Plazek, Polymer 42 (2001) 2555.
[25] Y. Tanaka, T. Yamamoto, J. Non-cryst. Solids 358 (2012) 1687.
[26] M.A. Debolt, A.J. Easteal, P.B. Macedo, C.T. Moynihan, J. Am. Ceram. Soc. 59 (1976) 16.
[27] J.A. Nelder, R. Mead, Comput. J. 7 (1965) 308.
[28] C. Alvalez, N.T. Correia, J.J. Moura Ramos, A.C. Fernandes, Polymer 41 (2000) 2907.
[29] A. Brunacci, J.M.G. Cowie, R. Ferguson, I.J. McEwen, Polymer 865 (1997) 38.